Thermal Science and Engineering Progress 37 (2023) 101578

Contents lists available at ScienceDirect

Thermal Science and Engineering Progress

journal homepage: www.elsevier.com/locate/tsep

An experimental study of oily wastewater treatment in a humidification–dehumidification system with bubble column humidifier

Elias Eder [a,*], Michael Cordin [b], Tung Pham [b], Dieter Brüggemann [c], Markus Preißinger [a]

[a] illwerke vkw Endowed Professorship for Energy Efficiency, Research Center Energy, Vorarlberg University of Applied Sciences, 6850 Dornbirn, Austria
[b] Research Institute of Textile Chemistry and Textile Physics, University of Innsbruck, 6850 Dornbirn, Austria
[c] Chair of Engineering Thermodynamics and Transport Processes (LTTT), Center of Energy Technology (ZET), University of Bayreuth, 95440 Bayreuth, Germany

ARTICLE INFO

Keywords:
Humidification–dehumidification
Bubble column humidifier
Air humidification
Oily wastewater
Bilge water

ABSTRACT

Vast amounts of oily wastewater are byproducts of the petrochemical and the shipping industry and to this day frequently discharged into water bodies either without or after insufficient treatment. To alleviate the resulting pollution, water treatment processes are in great demand. Bubble column humidifiers (BCHs) as part of humidification–dehumidification systems are predestined for such a task, since they are insensitive to different feed liquids, simple in design and have low maintenance requirements. While humidification in a bubble column has been investigated plentiful for desalination, a systematic investigation of oily wastewater treatment is missing in literature. We filled this gap by analyzing the treatment of an oil–water emulsion experimentally to derive recommendations for future design and operation of BCHs. Our humidity measurements indicate that the air stream is always saturated after humidification for a liquid height of only 10 cm. A residual water mass fraction of 3.5 wt% is measured after a batch run of six hours. Furthermore, continuous measurements show that an increase in oil mass fraction leads to a decrease in system productivity especially for high oil mass fractions. This decrease is caused by the heterogeneity of the liquid temperature profile. A lower liquid height mitigates this heterogeneity, therefore decreasing the heat demand and improving the overall efficiency. The oil content of the produced condensate is below 15 ppm, allowing discharge into various water bodies. The results of our systematic investigation prove suitability and indicate a strong future potential for the use of BCHs in oily wastewater treatment.

1. Introduction

Humidification–dehumidification (HDH) is a desalination technology to address water scarcity, particularly in arid and remote regions [1]. A lot of efforts are made to improve the efficiency and to reduce the associated cost of this process, including pressure variations [2], thermodynamic balancing [3,4], multi-stage setups [5,6] or the combination with heat pumps [7,8]. Although its efficiency is still somewhat limited, the importance of HDH is ever-growing due to (1) low maintenance requirements, (2) the ability to use low-grade and renewable thermal energy sources and (3) an insensitivity to various feed liquids [9,10]. This insensitivity indicates the potential of HDH to also treat oily wastewater.

Different industrial processes generate oily wastewater as a byproduct. Especially in the petrochemical industry [11] and in the hull of ocean-going vessels as bilge water [12], large quantities of oil-containing wastewater are generated. Pollution by oily wastewater is a serious issue and has multiple negative impacts on the environment and human health [13]. Centrifugal and gravitational separation, membrane processes [14–16] and electrocoagulation [17,18] as standalone processes or in combination are applied to treat oily wastewater. While air flotation has been used quite successfully for oily wastewater from the petrochemical industry [10], it is often inadequate for treating bilge water, because the bilge water is emulsified [19]. Membrane processes on the other hand, are widely applied for oily wastewater treatment, but are still somewhat limited due to insufficient understanding of the membrane fouling by emulsified oil [20]. Due to its unique advantages, HDH can be a promising candidate for treating different kinds of oily wastewater, including bilge water.

This process mimics the natural water cycle and consists of the humidification and subsequent dehumidification of a carrier gas, which is mostly air [21–24]. For the humidification part of this process, different designs have been tested and recommended, including spray towers [25], falling film evaporators [26] and packed bed towers [27].

Abbreviations: HDH, Humidification–Dehumidification; BCH, Bubble Column Humidifier; OAOW, Open-Air Open-Water

* Corresponding author.
E-mail address: elias.eder@fhv.at (E. Eder).

https://doi.org/10.1016/j.tsep.2022.101578
Received 9 August 2022; Received in revised form 19 October 2022; Accepted 21 November 2022
Available online 6 December 2022
2451-9049/© 2022 The Author(s). Published by Elsevier Ltd. This is an open access article under the CC BY license (http://creativecommons.org/licenses/by/4.0/).

Nomenclature

Acronyms

BCH	Bubble column humidifier
HDH	Humidification–dehumidification
OAOW	Open-air open-water

Subscripts

0	Initial, orifice
a	Air
b	Bottom
c	Condensate
calc	Calculated
cw	Cooling water
dh	Dehumidifier
emu	Oil–water emulsion
hum	Humidity sensor
i	Humidifier inlet
l	Liquid
max	Maximum
o	Humidifier outlet
oil	Oil
p	Probe
sol	Solvent
stp	Standard temperature and pressure
t	Top
tw	Tap water
v	Water vapor

Greek Symbols

β	Mass concentration of hydrocarbons (mg/l)
ω	Humidity ratio (kg_v/kg_a)
ϕ	Volume fraction (vol%)
τ	Relative transmittance (%)
$\tilde{\nu}$	Wavenumber (1/m)
ϵ	Efficiency (–)
φ	Relative humidity (%RH)

Physical Properties

$\dot{m}$	Mass flow (kg/s)
$\dot{Q}$	Heat flow (W)
c	Group extinction coefficient (m^2/kg)
d	Layer thickness (m)
E	Extinction (–)
F	Function (–)
H	Liquid height (m)
m	Mass (kg)
p	Pressure (Pa)
s	Standard deviation (–)
T	Temperature (°C)
t	Time (h)
T_λ	Transmittance (%)
V	Volume (m^3)
v	Velocity (m/s)
x	Independent variable (–)
Y	Mass fraction (wt%)

Additionally, bubble column humidifiers (BCHs) have frequently been proposed and investigated for HDH cycles [28–31]. In comparison with conventional humidifiers, they provide high heat and mass transfer, a low technological demand and do not encounter fouling [4,21]. Preißinger [32] investigated the accumulation of bilge water in an HDH-cycle with a BCH and gave evidence of the general working concept, but also reported a lack of fundamental understanding of the humidification of air in a bubble column. Thus, although BCHs are a potential candidate for treating oily wastewater, there are no comprehensive studies on this application.

The productivity of an HDH-system strongly relies on the degree of humidification and therefore on the amount of water evaporated. Because of that the humidity ratio at the humidifier outlet must be measured with high accuracy. Several studies have measured either full or close to saturation of the air stream directly at the BCH outlet using different kinds of humidity sensors [30,33,34]. However, studies show that humidity sensors are consistently covered with liquid droplets if installed directly at the humidifier outlet due to the high temperature and high relative humidity of the air stream. Consequently, the sensor indicates saturation of the air stream [35,36]. In a previous study [37], we managed to overcome this issue by installing a heating section directly at the outlet of the BCH. Our specified setup allowed us to gain a fundamental understanding of the humidification of air in a BCH for the desalination of seawater. In this study, we use the same setup to systematically investigate the humidification of air for treating oily wastewater.

For the first time, a comprehensive experimental investigation of the accumulation of a selected oil–water emulsion in a BCH is conducted in this study. With this study, we intend to address the evident lack of scientific studies with respect to this application. To this end, we conduct batch-wise and continuous measurements to better understand the behavior of the BCH in transient and steady state conditions. Our investigations include (1) a systematic determination of the outlet air state after humidification for the present liquid mixture, (2) an evaluation of the transient system behavior in batch-wise experiments and (3) a characterization of the impact of the oil mass fraction on the outlet air state in continuous experiments. To sum up, this study lays the foundation for treating oily wastewater with the HDH process and a BCH.

2. Methods and materials

Experimental test setup: The HDH test setup used for our experiments is depicted in Fig. 1 and consists of a humidifier, a dehumidifier and a heat source. The HDH-system is comprised of an open-water open-air cycle (OAOW) with heated liquid phase.

The BCH (1) consists of acrylic glass cylinders with an inner diameter of $d = 0.14$ m and stainless-steel parts as connectors. A fin and tube heat exchanger (2) is used as dehumidifier to cool the air stream below dew point temperature and condense the water vapor. The liquid height is measured continuously by a floater-based sensor (3) and is maintained using a dosage pump (4). For continuous mixing of the emulsion, we installed a magnetic stirrer (5). Preliminary measurements on our setup show that phase separation of the emulsion occurs, when not using the magnetic stirrer. The rate of rotation of the magnetic stirrer is set to 1000 rpm for all conducted measurements. Liquid temperature is controlled via resistance thermometer $T_{l,set}$ and heating cartridges (6). It is measured both at the bottom side of the liquid column $T_{l,b}$ (7) and at the top side of the liquid column $T_{l,t}$ (8) using resistance thermometers. The inlet air is taken from a pressurized air system, controlled by a mass flow controller (9) and then dispersed into fine bubbles using a sparger module. A laser cut sparger plate made from acrylic glass with an orifice diameter of $d_0 = 0.001$ m is mounted on the sparger module. Air temperature is measured at the humidifier inlet T_i (10), at the humidifier outlet T_o (11) and at the dehumidifier outlet $T_{dh,o}$ (12) using resistance thermometers. Furthermore, we installed a heating line (13) after the humidifier outlet for lowering relative humidity of the outlet air stream while maintaining a constant humidity ratio. Consequently, condensation of water droplets on the humidity

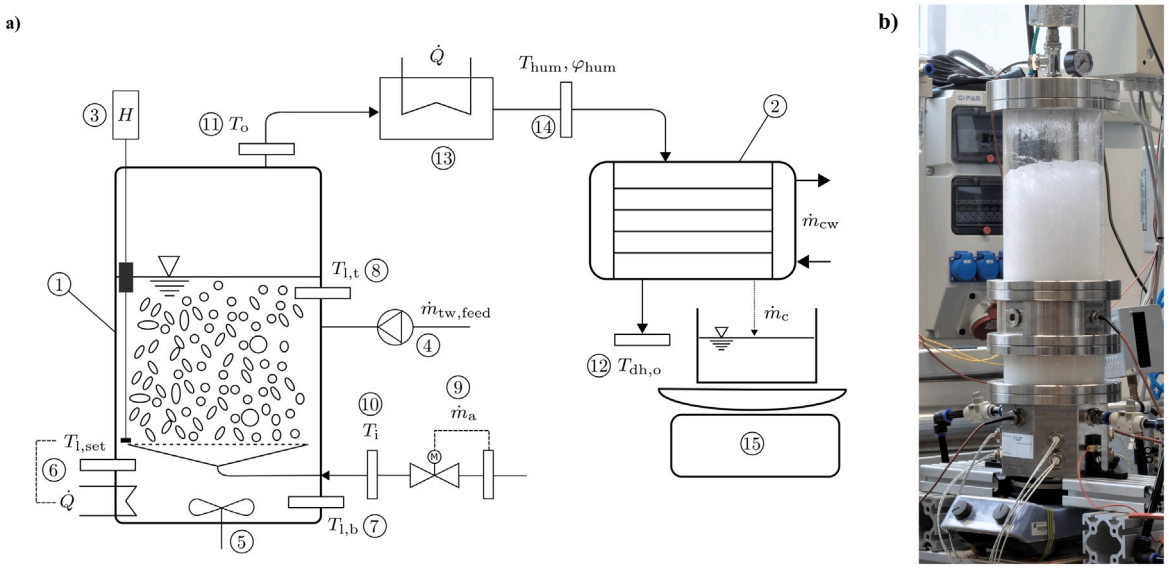

Fig. 1. (a) HDH process scheme and (b) photograph of the BCH without thermal insulation.

sensor is prevented, enabling accurate measurements of the outlet air state [37]. Thermal insulation is applied to the BCH and all parts before the heating line to minimize heat loss to the environment. After the heating line, temperature and relative humidity of the air are measured by a capacitive humidity sensor (T_{hum}, φ_{hum} (14)). Cooling water is cycled separately in the dehumidifier, to cool the air stream and condense the water vapor. The produced condensate is continuously collected and weighed by a digital scale (15). All relevant data are logged in intervals of 30 seconds throughout the measurement periods.

The current mass flow of water vapor evaporated $\dot{m}_{\mathrm{v}}(t)$ is calculated using Eq. (1), where $\dot{m}_{\mathrm{a}}$ is air mass flow and $\omega_{\mathrm{o}}(t)$ and $\omega_{\mathrm{i}}(t)$ are humidity ratios at the humidifier outlet and inlet, respectively.

$$\dot{m}_{\mathrm{v}}(t) = \dot{m}_{\mathrm{a}} \cdot \left[\omega_{\mathrm{o}}(t) - \omega_{\mathrm{i}}(t)\right] \tag{1}$$

The inlet air is dried in a demister unit and should therefore not contain water vapor. To check this assumption, the air stream humidity ratio at the humidifier inlet is measured once in a preliminary measurement run and determined to be $\omega_{\mathrm{i}} = 0.2\ \mathrm{g_v/kg_a}$. As changes to this value are negligible during operation, it is considered constant for all measurements.

As compared to previous experimental studies of the humidification in bubble columns [29,30], we have added an additional heating line before the humidity sensor. This allows us to accurately measure outlet air conditions. To determine the air state after humidification, humidity ratio and relative humidity need to be calculated. The air stream humidity ratio is calculated using Eq. (2) with relative humidity φ, the atmospheric pressure p_{atm} of 101325 Pa and saturation pressure p_{s}, which is calculated for the respective temperatures using the Antoine equation:

$$\omega(\varphi, T) = 0.622 \cdot \frac{\varphi \cdot p_{\mathrm{s}}(T)}{p_{\mathrm{atm}} - \varphi \cdot p_{\mathrm{s}}(T)} \tag{2}$$

Relative humidity φ is calculated using Eq. (3), where ω is humidity ratio, p_{atm} is the atmospheric pressure and p_{s} is saturation vapor pressure:

$$\varphi(\omega, T) = \frac{\omega \cdot p_{\mathrm{atm}}}{(0.622 + \omega) \cdot p_{\mathrm{s}}(T)} \tag{3}$$

Eqs. (2) and (3) are used in the batch-wise experiments and the continuous experiments to determine the air state after humidification. The detailed method is described in the following subsections.

Batch-wise experiments: To conduct the batch experiments, a specified liquid mixture is prepared and filled into the humidifier.

Table 1
Emulsion constituents.

Constituent	Name	Amount g
Industrial white oil	Petro Canada Purity FG WO 35	2750
Tap water	–	2206
Emulsifier	SDBS	11
Anti-foaming agent	Rimagents-L	27

Throughout the batch measurements, the reduction in liquid height caused by the evaporation of water vapor is not compensated. The liquid height in the bubble column is therefore continuously decreasing. Eq. (2) is used to calculate the humidity ratio ω_{hum} based on the measured temperature T_{hum} and relative humidity φ_{hum} of the humidity sensor. Eq. (3) is then used to calculate relative humidity of the air for the following assumptions:

- **Assumption 1:** The air is assumed to be saturated and at the top side liquid temperature $T_{\mathrm{l,t}}$.
- **Assumption 2:** The air is assumed to be saturated and at the humidifier outlet temperature T_{o}.

Fig. 2 indicates the sensor positions and relative humidities to be calculated, respectively. We placed the resistance thermometer to control the heating cartridges' power output $T_{\mathrm{l,set}}$ at the top side of the liquid (Fig. 2). Preliminary measurements have shown that this sensor placement is necessary for high oil mass fractions ($Y_{\mathrm{oil}} > 65$ wt%) to prevent an insufficiently low top side liquid temperature because of the high liquid viscosity. Two batch-wise measurement runs are conducted, with tap water and a specific oil–water emulsion, respectively. The tap water run is conducted for validation purposes of the measurement method.

The oil–water emulsion is prepared according to Table 1. Sodium dodecylbenzenesulfonate (SDBS) is used as an emulsifier. Rimagents-L is additionally added as an anti-foaming agent for preventing foam formation. The batch-wise experiment is conducted at an initial oil mass fraction of about $Y_{\mathrm{oil,0}} = 55$ wt%, attempting to reach an oil mass fraction of $Y_{\mathrm{oil}} = 100$ wt% by removing the entire water phase from the liquid mixture.

The overall amount of water vapor evaporated $m_{\mathrm{v,calc}}(t)$ is determined using Eq. (4) by integration of the current mass flow of water

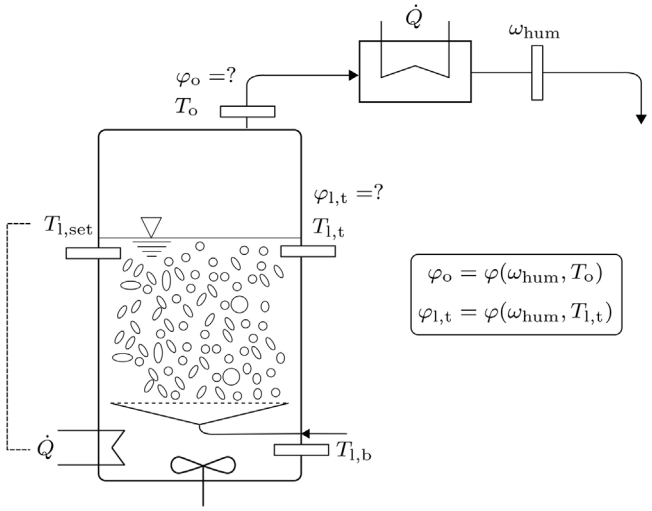

Fig. 2. Bubble column humidifier with sensor positions for calculations of the outlet air state.

vapor evaporated (as given by Eq. (1)):

$$m_{\mathrm{v,calc}}(t) = \int_0^t \dot{m}_{\mathrm{v}} \cdot dt \tag{4}$$

The current oil mass fraction is calculated by Eq. (5) using the initial masses of oil and tap water m_{oil} and m_{tw} as well as the overall amount of water vapor evaporated at a certain time $m_{\mathrm{v,calc}}(t)$:

$$Y_{\mathrm{oil}}(t) = \frac{m_{\mathrm{oil}}}{m_{\mathrm{oil}} + m_{\mathrm{tw}} - m_{\mathrm{v,calc}}(t)} \cdot 100\ \mathrm{wt\%} \tag{5}$$

For all calculations of the oil mass fraction, the emulsifier and anti-foaming agent are neglected, as they only account for 0.5 wt% of the entire emulsion. The water mass fraction can then be calculated as

$$Y_{\mathrm{tw}}(t) = 100\ \mathrm{wt\%} - Y_{\mathrm{oil}}(t). \tag{6}$$

The described batch run will be conducted either until the entire water phase is removed or until the process stops working efficiently. Subsequently to this measurement, we collect a liquid probe of the residual emulsion for analysis. The water mass fraction of this liquid probe is characterized using Karl Fischer titration, to cross-verify the calculated result based on the measurement of the humidity sensor.

Water content determination: To determine the water content in the residual emulsion of the batch-wise experiment, we use Coulometric Mettler Toledo Karl Fischer titrator C30. The general working principle of a coulometric Karl Fischer titration is as follows:

1. The titration cell consists of an anode solution and a smaller compartment with the cathode. An ion-permeable membrane separates the anode solution and the cathode.
2. The liquid to be measured is given into the titration solution drop-wise. By applying an electric current, a reaction takes place that consumes water. This reaction will eventually stop once the available water has been used up.
3. The reaction time is measured and used to determine the water content of the probe, based on the probe volume dropped into the titration solution.

Continuous experiments: For the continuous measurement runs, a parametric variation of the oil mass fraction is conducted. The sensor placement within the experimental setup is similar to the one depicted in Fig. 2, except for the resistance thermometer to control the power output of the heating cartridges $T_{\mathrm{l,set}}$, which is mounted at the bottom side of the liquid column instead of at the top side. To have a constant liquid height for various mass concentrations of oil, the emulsions are prepared to a total emulsion volume of $V_{\mathrm{emu}} = 3.3$ l. The volume fraction of oil is then varied between $\phi_{\mathrm{oil}} = 0$ vol% and $\phi_{\mathrm{oil}} = 65$ vol%, corresponding to oil mass fractions between $Y_{\mathrm{oil}} = 0$ wt% and $Y_{\mathrm{oil}} = 61.6$ wt%. For this measurement series, liquid height is maintained constant throughout the measurements. The liquid height is maintained by continuously feeding tap water using the dosage pump (4). As water vapor is extracted almost exclusively with the air stream, variations in the oil mass fraction are negligible. A typical test run is conducted as follows:

1. The oil–water emulsion is prepared to the designated volume fraction of oil and filled into the humidifier.
2. The liquid temperature, the air mass flow and the liquid height are set and maintained throughout the measurement run. The set benchmark values are $T_{\mathrm{l,set}} = 70$ °C, $\dot{m}_{\mathrm{a}} = 1.41$ kg/h ($v_{\mathrm{a}} = 2$ cm/s) and $H = 100$ mm.
3. As soon as a steady state is reached, indicated by a negligible change in air outlet temperature, all sensor data are logged for a duration of 60 min.

Throughout the measurements, samples are taken to determine the oil content of the produced condensate. The procedure is described in the following subsection.

Oil content determination: To determine the oil content of the produced condensate, FTIR-spectroscopy is used on selected samples. For the preparation of the samples, liquid–liquid extraction is conducted with trichlorotrifluoroethane (CFC-113) as a solvent. The method for measuring oil content in water samples is described in DIN-Norm 38409 part 18 [38].

The transmittance T_λ is measured and evaluated at three distinct wavenumbers $\tilde{\nu}$ representing CH-groups. The individual CH-groups are:

- $\tilde{\nu} = 3020$ 1/cm: CH-group
- $\tilde{\nu} = 2929$ 1/cm: CH_2-group
- $\tilde{\nu} = 2962$ 1/cm: CH_3-group

The relative transmittance τ is calculated as the ratio of the transmittance of the sample and the transmittance of the pure solvent:

$$\tau = \frac{T_\lambda}{T_{\lambda,\mathrm{sol}}} \tag{7}$$

Extinction E is calculated based on the relative transmittance using Eq. (8):

$$E = -log(\tau) \tag{8}$$

The mass concentration of hydrocarbons β can ultimately be calculated as

$$\beta = \frac{1.3 \cdot V_{\mathrm{sol}} \cdot \left(\frac{E_1}{c_1} + \frac{E_2}{c_2} + \frac{E_3}{c_3}\right)}{V_{\mathrm{p}} \cdot d}, \tag{9}$$

where β is denoting the mass concentration of hydrocarbons, E_1, E_2 and E_3 the extinction values of the respective CH-groups, c_1, c_2 and c_3 the extinction coefficients of the respective CH-groups, V_{sol} and V_{p} the volume of solvent and probe, respectively and d is denoting the layer thickness of the sample.

Error analysis: For all of the conducted measurements, the measurement uncertainty is evaluated. The installed sensors and instruments are listed in Table 2 with their individual range and uncertainty.

For figures that display absolute values, error bars indicate the uncertainty of the measurement instruments. For derived values, error propagation is used to calculate the standard deviation (see Eq. (10)):

$$s_{\mathrm{F}} = \sqrt{\sum_{\mathrm{i}} \left(\frac{\partial F}{\partial x_{\mathrm{i}}} \cdot s_{\mathrm{i}}\right)^2} \tag{10}$$

with x_{i} denoting independent variables with their respective standard deviation s_{i} and function sensitivity $\partial F / \partial x_{\mathrm{i}}$.

Table 2
Sensors, measurement ranges and uncertainties.

Sensor type	Measurement range	Uncertainty
PT1000 thermometer class B (6, 7, 8, 10, 11, 12)	0–100 °C	$\pm[0.3 + 0.005 \cdot T]$ °C
PT1000 thermometer class AA (14)	0–180 °C	$\pm[0.1 + 0.0017 \cdot T]$ °C
Capacitive humidity sensor (14)	0–100 %RH	$\pm[1 + 0.007 \cdot \varphi]$ %RH
Floater based liquid height sensor (3)	0–500 mm	±0.5 mm
Mass flow meter (9)	0–10 m^3_{stp}/h	±0.01 m^3_{stp}/h
Digital scale (15)	0–3100 g	±0.01 g

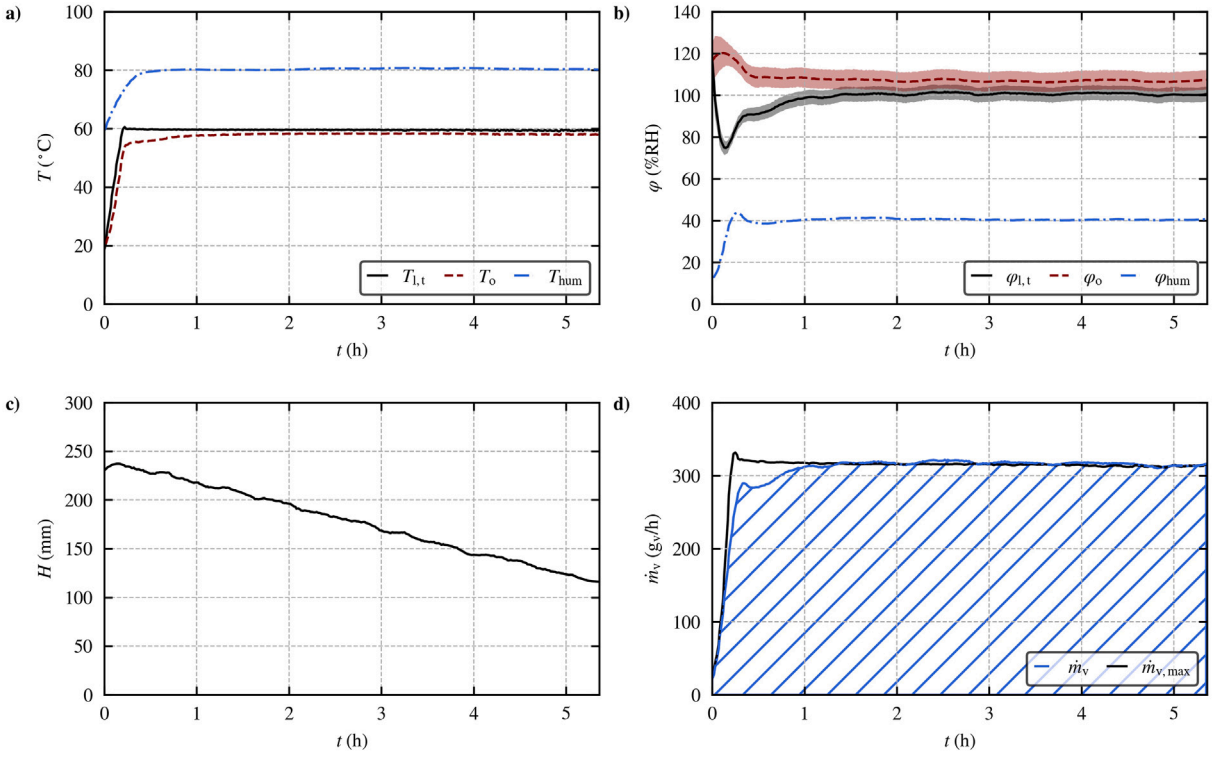

Fig. 3. Tap water batch run; (a) system temperatures, (b) relative humidities, (c) liquid height and (d) amount of water vapor evaporated with dependence on time, $T_{l,set}$ = 60 °C, $\dot{m}_a$ = 2.12 kg/h (v_a = 3 cm/s) and m_0 = 5217 g.

3. Results and discussion

Batch-wise experiments: In Fig. 3, the results with tap water as liquid phase are visualized. These include (a) system temperatures, (b) calculated relative humidities, (c) liquid height and (d) amount of water vapor evaporated with respect to measurement time. For better visibility and comparison, measurement uncertainties are only indicated for $\varphi_{l,t}$ and φ_o in Fig. 3(b) (as indicated by the semi-transparent areas). As these reflect the uncertainties of the respective measurement instruments, they can be considered systematic errors. To reduce the noise on certain time-dependent signals, a Savitzky–Golay filter [39] is applied to selected data series.

In steady state, the air temperature at the humidifier outlet T_o lies slightly below the top side liquid temperature $T_{l,t}$ (see Fig. 3(a)). This indicates a high heat transfer from the liquid column to the air stream. It is noteworthy that the liquid temperature profile in the BCH is very homogeneous for the operation with tap water. Consequently, the top side liquid temperature and the bottom side liquid temperature deviate by only 0.2 K on average. The air temperature, as measured by the humidity sensor, is at approximately T_{hum} = 80 °C in steady state with the heating line temperature set to 120 °C.

The relative humidity of the air stream is at approximately φ_{hum} = 40 %RH during steady state operation. This indicates that condensation on the humidity sensor is no longer an issue and that an accurate measurement of the air state using a humidity sensor is possible. Corresponding to the measured humidity ratio ω_{hum}, the relative humidity of the air would need to be at a 100 %RH, if the air was at top side liquid temperature $T_{l,t}$ and above 100 %RH, therefore supersaturated and containing liquid droplets, if the air was at humidifier outlet temperature T_o, according to Fig. 3(b). This concludes that the air stream is saturated directly at the liquid surface for the operation with tap water.

The decrease in liquid height is linear in steady state operation, as can be seen in Fig. 3(c). This is also reasonable, as the amount of water vapor evaporated $\dot{m}_v$ is constant over this period.

By integrating $\dot{m}_v$, the overall amount of water vapor evaporated $m_{v,calc}(t)$ can be computed (see Eq. (4)). This integration is visualized in Fig. 3(d) by the dashed area. The amount of water vapor evaporated $\dot{m}_v$ strongly increases at the beginning of the measurement, when the HDH system is heating up. Once system temperatures reach a steady state, the amount of water vapor evaporated stays constant as well. In steady state, it corresponds to the maximum value $\dot{m}_{v,max}$, which is calculated with the assumption that the air stream reaches the top side liquid temperature and is in saturated state.

Fig. 4 shows the results of the accumulation of an oil–water emulsion including (a) system temperatures, (b) oil mass fraction, (c) liquid height and (d) amount of water vapor evaporated. The current oil mass fraction $Y_{oil}(t)$ and water mass fraction $Y_{tw}(t)$ are derived from Eqs. (5) and (6) using the overall amount of water vapor evaporated. The uncertainties of the oil mass fraction Y_{oil} and of the water mass fraction Y_{tw} are determined via Eq. (10) and also visualized in Fig. 4(b)

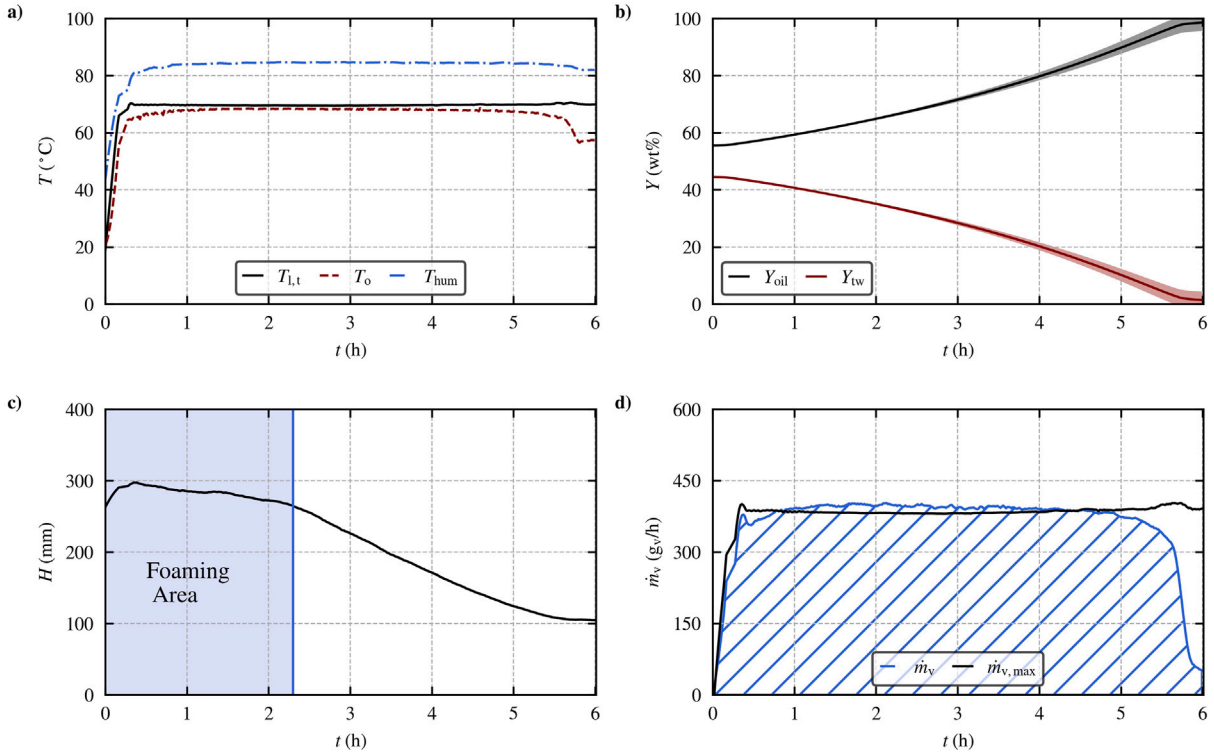

Fig. 4. Oil–water emulsion batch run; (a) system temperatures, (b) oil and water mass fraction, (c) liquid height and (d) amount of water vapor evaporated with dependence on time, $T_{l,set} = 70$ °C, $\dot{m}_a = 1.41$ kg/h ($v_a = 2$ cm/s) and $m_0 = 4994$ g.

as semi-transparent areas. Savitzky–Golay filtering [39] is applied to reduce the noise of selected time-dependent signals.

According to Fig. 4, the humidifier outlet temperature T_o is gradually reaching a steady state and then remaining constant for the majority of the measurement duration. However, at approximately 5.5 h, there is a drop in humidifier outlet temperature. Correspondingly, the air humidity ratio ω_{hum} drops at an oil mass fraction of approximately $Y_{oil} = 96$ wt% (see Fig. 4(d)). This temperature drop can be explained by the drop in humidity ratio, as a humid air stream has a higher thermal mass and is cooled less in comparison with a low humidity air stream.

Even though anti-foaming agent is used to prevent foam formation, such formation occurred, especially for low oil mass fractions. This formation affects the decrease in liquid height. In the foaming area (see Fig. 4(c)), the reduction in liquid height is partially compensated by a reduction in foam volume. The reduction in liquid height reaches its maximum once the entire foam disappeared. That point was determined by taking images of the bubbly flow at regular intervals to be at approximately 2.3 h and is indicated by the vertical line. At the end of the batch experiment, the liquid height is not reduced anymore and the measured humidity ratio at the humidifier outlet drops to the initial value.

Table 3 lists the overall amounts of water vapor evaporated $m_{v,calc}$, the measured liquid weight reduction Δm in the humidifier and the amount of condensate m_c collected in the dehumidifier. For the tap water run, liquid weight of the batch is measured with a digital scale at the beginning and the end of the measurement run to calculate the weight difference. For the oil–water emulsion, the initial amount of water is already known from preparing the emulsion.

The results based on Table 3 are summarized as follows:

- **The humidity measurement has a relative error of less than 5 %**: The overall amount of water vapor evaporated underestimates the liquid weight reduction by only 4.1% for the tap water run. A small underestimation is reasonable and potentially caused by weighing losses due to residual water in the humidifier after the experiments and due to an increased time period for the humidity sensor to reach a steady state value, as can be seen in Fig. 3(d).
- **The produced condensate in the dehumidifier is 10 to 20 wt% lower than the amount of water vapor evaporated:** A dehumidifier efficiency lower than $\varepsilon_{dh} = 1$ leads to this behavior. This indicates that the productivity of the whole HDH-system is not suitable to characterize the humidification process unless dehumidifier losses are accounted for.
- **For this study, the residual water content in the oil–water emulsion is between $Y_{tw} = 0$ wt% and $Y_{tw} = 4.5$ wt%**: This value is derived from the oil mass fraction that is calculated using Eq. (5) and the overall mass of water vapor evaporated $m_{v,calc}(t)$. Since the measurement uncertainties and error propagation do not allow for a more accurate estimation, this result will be cross verified using Karl Fischer titration.

Table 3
Measurement results.

Liquid phase	Δm g	$m_{v,calc}$ g	m_c g
Tap water	1704	1633 ± 68	1411
Oil–water emulsion	2206 (m_0)	2167 ± 89	1944

For the batch-wise measurement run with the oil–water emulsion as the liquid phase, selected probes are taken and depicted for optical inspection, as seen in Fig. 5.

The initial oil–water emulsion in Fig. 5(a) shows a phase separation that is not occurring in operation due to magnetic stirring. The prepared emulsion is an oil-in-water emulsion, thus water is the continuous phase. The produced condensate in Fig. 5(b) looks highly pure, there is no turbidity. Still, there are minimal traces of oil visible on the surface. The emulsified residue, as seen in Fig. 5(c), is highly viscous after removing the majority of the initial water phase.

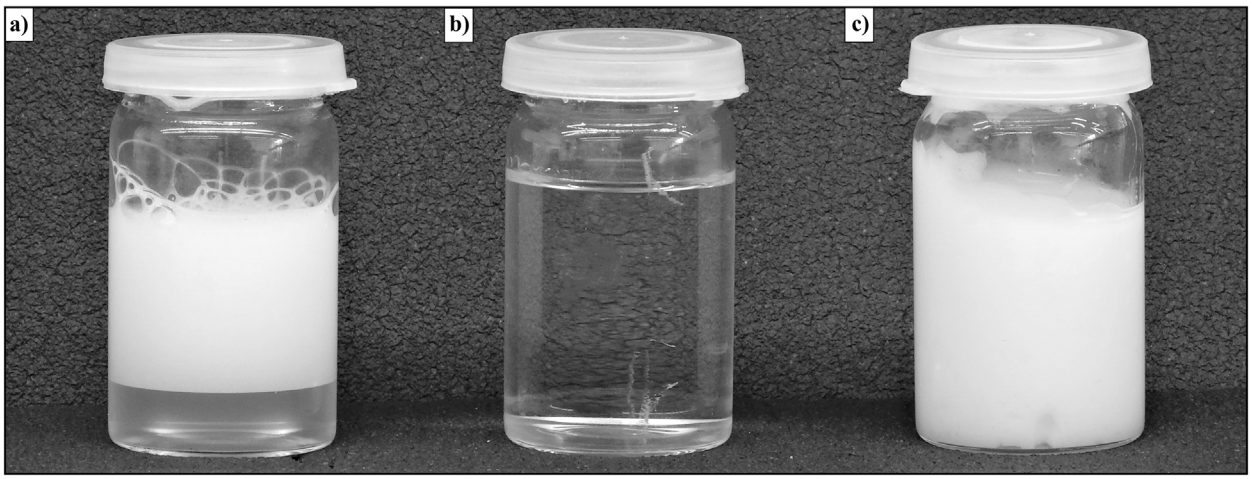

Fig. 5. Liquid probes of (a) the initial emulsion with visible phase separation, (b) the produced condensate and (c) the accumulated and emulsified oil phase.

Karl Fischer titration: To measure the terminal water mass fraction in the residual emulsion and to validate the calculated amount of water vapor evaporated, Karl Fischer titration is applied to a liquid probe (see Fig. 5(c)). The residual water mass fraction is determined to be $Y_{tw} = 3.5$ wt%. This result agrees well with the residual mass fraction determined by the calculations previously described ($Y_{tw} = 0$ wt% to $Y_{tw} = 4.5$ wt% terminal water mass fraction).

Continuous experiments: In Fig. 6 the results of the continuous measurement series conducted with the oil–water emulsion are displayed. In this figure, (a) system temperatures, (b) selected temperature differences and (c) humidity ratios are shown. The selected temperature differences are denoted as follows:

- ΔT_1: Temperature difference between the top side liquid temperature $T_{l,t}$ and the bottom side liquid temperature $T_{l,b}$ (axial temperature profile of the liquid column)
- ΔT_2: Temperature difference between the top side liquid temperature $T_{l,t}$ and the humidifier outlet temperature T_o (cooling due to radial heat losses)

The humidity ratio of air at top side liquid temperature $\omega_{l,t}$, as shown in Fig. 6(c), is calculated using Eq. (2), with the assumption of saturated air at the top side liquid temperature $T_{l,t}$ and compared to the measured humidity ratio ω_{hum}.

As can be seen in Fig. 6(a), all system temperatures are almost constant for oil mass fractions of up to $Y_{oil} = 40$ wt% and sharply decreasing for higher oil mass fractions. This indicates that the magnetic stirring is successful only up to a certain liquid viscosity. For lower liquid viscosities, the investigated temperatures are almost constant, whereas for higher liquid viscosities the magnetic stirring is insufficient, resulting in a temperature drop and a more heterogeneous temperature profile. The temperature difference ΔT_1 is therefore also increasing exponentially for high oil mass fractions according to Fig. 6(b). As the liquid is heated from the bottom side of the humidifier, it is reasonable that the bottom side liquid temperature $T_{l,b}$ is higher than the top side liquid temperature $T_{l,t}$ for all investigated measurements. On the other hand, the temperature difference ΔT_2 between the top side liquid temperature and the humidifier outlet temperature is unaffected by changes in the oil mass fraction, which is also reasonable.

In Fig. 6(c), there is a remarkable agreement between the measured humidity ratio of the humidity sensor ω_{hum} and the calculated humidity ratio $\omega_{l,t}$ based on the assumption of saturated air at the top side liquid temperature. Independently of the oil mass fraction, it follows that the air stream is always saturated at the top side liquid temperature for the investigated conditions. Furthermore, the saturation pressure of the oil–water emulsion must be close to the saturation pressure of pure water, as there is no significant deviation between the two values of humidity ratio even for high oil mass fractions. This is in accordance with a study of Aranberri et al. [40], who stated that the evaporation from water as the continuous phase of an oil–water-emulsion is identical to the evaporation from pure water.

Table 4
Relative transmittance and mass concentration of hydrocarbons.

Probe	τ_{CH} –	τ_{CH_2} –	τ_{CH_3} –	β mg/l
$Y_{oil} = 20$ wt%	0.984	0.658	0.756	4.55
$Y_{oil} = 40$ wt%	0.959	0.553	0.677	5.44
$Y_{oil} = 60$ wt%	0.967	0.624	0.731	5.73

Oil content of product: The residual oil content of the product is investigated using a Bruker Invenio FTIR spectrometer. Three samples of the produced condensate are taken at oil mass fractions $Y_{oil} = 20$ wt%, $Y_{oil} = 40$ wt% and $Y_{oil} = 60$ wt% of the oil–water emulsion in the humidifier.

In Fig. 7, the transmittance T_λ of the selected samples and of the pure solvent is shown with dependence on the wavenumber $\tilde{\nu}$.

It can be seen that the transmittance T_λ of the samples after extraction is significantly lower than that of the pure solvent for the CH_2-group and the CH_3-group. The relative transmittances τ and the resulting mass concentration of hydrocarbons are given in Table 4 for every measured sample.

Table 4 shows no significant trend between the oil mass fraction of the oil–water emulsion in the BCH and the mass concentration of hydrocarbons in the produced condensate. However, for all samples investigated, the mass concentration of hydrocarbons is below the discharge limit of 15 ppm, regulated by MARPOL Annex I [19]. Therefore, the produced condensate is viable to be discharged into various water bodies.

4. Conclusion

The accumulation of an oil–water emulsion within an HDH-cycle with BCH is investigated to gain a better understanding of the humidification process for treatment of oily wastewater. Batch-wise experiments and continuous experiments are conducted to investigate the transient system behavior and the impact of the oil mass fraction. The main results of this study are summarized as follows:

- It is empirically shown that an oil–water emulsion can be accumulated in a BCH. The residual water mass fraction has been determined to be 3.5 wt%, so evidently, the majority of the water within the emulsion has been evaporated.

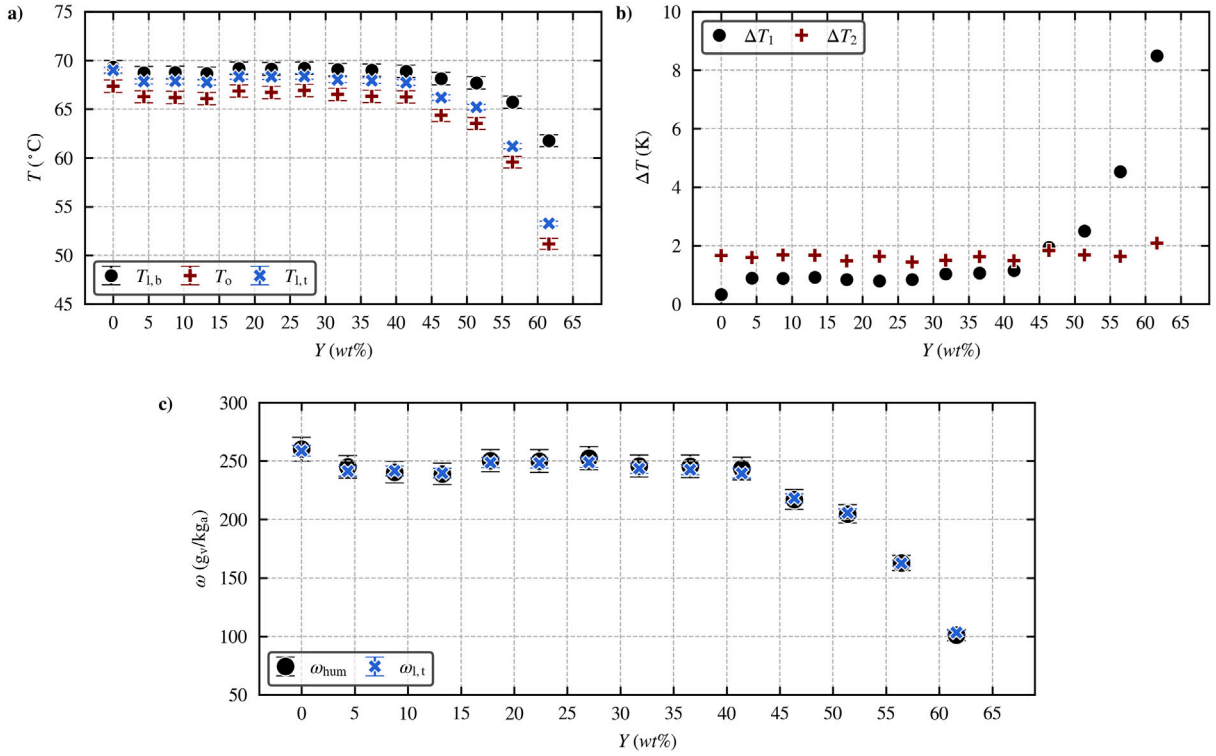

Fig. 6. Continuous measurement series with the oil–water emulsion; (a) system temperatures, (b) selected temperature differences and (c) humidity ratios measured by the humidity sensor (14, ω_{hum}) and calculated using the top side liquid temperature (8, $\omega_{l,t}$), $T_{l,set} = 70$ °C, $\dot{m}_a = 1.41$ kg/h ($v_a = 2$ cm/s) and $H = 100$ mm.

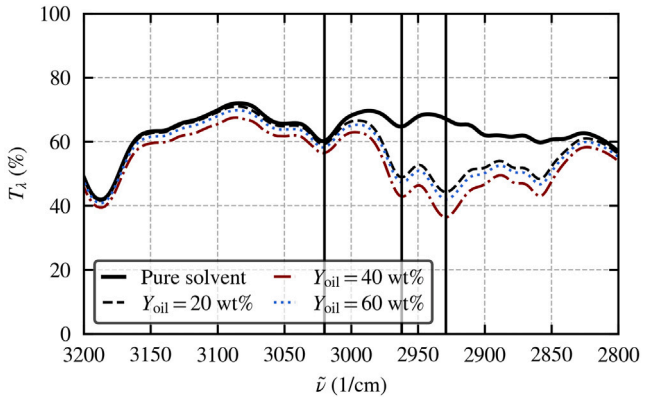

Fig. 7. Transmittance of condensate probes after extraction and pure solvent with respect to wavenumber.

- For all investigated measurements, the air stream is shown to be in a saturated state and at the top side liquid temperature after humidification. The empirical proof of this has been enabled by installing a heating line before the humidity sensor preventing droplet formation.
- An increase in oil mass fraction negatively impacts the system productivity. This is caused by an increase in liquid viscosity, leading to a highly heterogeneous axial temperature profile within the bubble column. It is recommended, to either enable sufficient mixing of the liquid column or to reduce the liquid height altogether. To improve the efficiency, the liquid temperature profile has to be maintained as homogeneous as possible.
- For all investigated samples, the oil content is below the discharge limit of 15 ppm, allowing discharge of the product of this process.

We therefore proved the general suitability of the HDH-process with a BCH to treat oil–water emulsions. Based on our first holistic investigation, an HDH-system with BCH shows promising future potential for the treatment of oily wastewater.

CRediT authorship contribution statement

Elias Eder: Conceptualization, Methodology, Investigation, Writing – original draft, Visualization. **Michael Cordin:** Investigation, Writing – review & editing. **Tung Pham:** Resources, Writing – review & editing. **Dieter Brüggemann:** Supervision, Writing – review & editing. **Markus Preißinger:** Supervision, Conceptualization, Project administration, Funding acquisition, Writing – review & editing.

Declaration of competing interest

The authors declare that they have no known competing financial interests or personal relationships that could have appeared to influence the work reported in this paper.

Data availability

Data will be made available on request.

Acknowledgment

This work is financed by the Austrian Science Fund (FWF) via project grant number P31103.

References

[1] A.S.A. Mohamed, M.S. Ahmed, H.M. Maghrabie, A.G. Shahdy, Desalination process using humidification–dehumidification technique: A detailed review, Int. J. Energy Res. (2020) 1–52, http://dx.doi.org/10.1002/er.6111.

[2] H. Liu, M.H. Sharqawy, Experimental performance of bubble column humidifier and dehumidifier under varying pressure, Int. J. Heat Mass Transfer 93 (2016) 934–944, http://dx.doi.org/10.1016/j.ijheatmasstransfer.2015.10.040.
[3] M.S. Elzayed, M. Ahmed, M.A. Antar, M.H. Sharqawy, S.M. Zubair, The impact of thermodynamic balancing on the performance of a humidification dehumidification desalination system, Therm. Sci. Eng. Prog. 21 (2021) 100794, http://dx.doi.org/10.1016/j.tsep.2020.100794.
[4] G.P. Narayan, M.H. Sharqawy, E.K. Summers, J.H. Lienhard, S.M. Zubair, M.A. Antar, The potential of solar-driven humidification–dehumidification desalination for small-scale decentralized water production, Renew. Sustain. Energy Rev. 14 (4) (2010) 1187–1201, http://dx.doi.org/10.1016/j.rser.2009.11.014.
[5] H.M. Abd-ur Rehman, F.A. Al-Sulaiman, A novel design of a multistage stepped bubble column humidifier for the humidification of air, Appl. Therm. Eng. 120 (2017) 530–536, http://dx.doi.org/10.1016/j.applthermaleng.2017.04.021.
[6] G. Wu, H. Zheng, X. Ma, C. Kutlu, Y. Su, Experimental investigation of a multistage humidification-dehumidification desalination system heated directly by a cylindrical Fresnel lens solar concentrator, Energy Convers. Manage. 143 (2017) 241–251, http://dx.doi.org/10.1016/j.enconman.2017.04.011.
[7] Y. Zhang, H. Zhang, W. Zheng, S. You, Y. Wang, Numerical investigation of a humidification-dehumidification desalination system driven by heat pump, Energy Convers. Manage. 180 (2019) 641–653, http://dx.doi.org/10.1016/j.enconman.2018.11.018.
[8] Y. Zhang, C. Zhu, H. Zhang, W. Zheng, S. You, Y. Zhen, Experimental study of a humidification-dehumidification desalination system with heat pump unit, Desalination 442 (2018) 108–117, http://dx.doi.org/10.1016/j.desal.2018.05.020.
[9] Y. Ghalavand, M.S. Hatamipour, A. Rahimi, A review on energy consumption of desalination processes, Desalin. Water Treat. (2014) 1–16, http://dx.doi.org/10.1080/19443994.2014.892837.
[10] P. Gao, M. Zhang, Y. Du, B. Cheng, D. Zhang, Study on bubble column humidification and dehumidification system for coal mine wastewater treatment, Water Sci. Technol. 77 (7) (2018) 1909–1919, http://dx.doi.org/10.2166/wst.2018.072.
[11] J. Coca, G. Gutiérrez, J. Benito, Treatment of oily wastewater, in: J. Coca-Prados, G. Gutiérrez-Cervelló (Eds.), Water Purification and Management, Dordrecht, 2011, pp. 1–55.
[12] P. Tiselius, K. Magnusson, Toxicity of treated bilge water: The need for revised regulatory control, Mar. Pollut. Bull. 114 (2) (2017) 860–866, http://dx.doi.org/10.1016/j.marpolbul.2016.11.010.
[13] L. Yu, M. Han, F. He, A review of treating oily wastewater, Arab. J. Chem. 10 (2017) 1913–1922, http://dx.doi.org/10.1016/j.arabjc.2013.07.020.
[14] M. Tomaszewska, A. Orecki, K. Karakulski, Treatment of bilge water using a combination of ultrafiltration and reverse osmosis, Desalination 185 (1–3) (2005) 203–212, http://dx.doi.org/10.1016/j.desal.2005.03.078.
[15] M. Gryta, Bilge water separation by membrane distillation, Sep. Purif. Technol. 237 (116332) (2020) 1–10, http://dx.doi.org/10.1016/j.seppur.2019.116332.
[16] K. Karakulski, W.A. Morawski, J. Grzechulska, Purification of bilge water by hybrid ultrafiltration and photocatalytic processes, Sep. Purif. Technol. 14 (1) (1998) 163–173, http://dx.doi.org/10.1016/S1383-5866(98)00071-9.
[17] M. Asselin, P. Drogui, S.K. Brar, H. Benmoussa, J. Blais, Organics removal in oily bilgewater by electrocoagulation process, J. Hard Mater. 151 (2) (2008) 446–455, http://dx.doi.org/10.1016/j.jhazmat.2007.06.008.
[18] Y. Bian, Z. Ge, C. Albano, F.L. Lobo, Z.J. Ren, Oily bilge water treatment using DC/AC powered electrocoagulation, Environ. Sci.: Water Res. Technol. 5 (10) (2019) 1654–1660, http://dx.doi.org/10.1039/C9EW00497A.
[19] J. Church, J.G. Lundin, D. Diaz, D. Mercado, M.R. Willner, W. Lee, D.M. Paynter, Identification and characterization of bilgewater emulsions, Sci. Total Environ. 691 (2019) 981–995, http://dx.doi.org/10.1016/j.scitotenv.2019.06.510.
[20] H.J. Tanudjaja, C.A. Hejase, V.V. Tarabara, A.G. Fane, J.W. Chew, Membrane-based separation for oily wastewater: A practical perspective, Water Res. 156 (2019) 347–365, http://dx.doi.org/10.1016/j.watres.2019.03.021.
[21] M. Faegh, P. Behnam, M.B. Shafii, A review on recent advances in humidification-dehumidification (HDH) desalination systems integrated with refrigeration, power and desalination technologies, Energy Convers. Manage. 196 (2019) 1002–1036, http://dx.doi.org/10.1016/j.enconman.2019.06.063.
[22] D.U. Lawal, N.A. Qasem, Humidification-dehumidification desalination systems driven by thermal-based renewable and low-grade energy sources: A critical review, Renew. Sustain. Energy Rev. 125 (2020) 109817, http://dx.doi.org/10.1016/j.rser.2020.109817.
[23] A. Kasaeian, S. Babaei, M. Jahanpanah, H. Sarrafha, A. Sulaiman Alsagri, S. Ghaffarian, W.-M. Yan, Solar humidification-dehumidification desalination systems: A critical review, Energy Convers. Manage. 201 (112129) (2019) 1–26, http://dx.doi.org/10.1016/j.enconman.2019.112129.
[24] K. Srithar, T. Rajaseenivasan, Recent fresh water augmentation techniques in solar still and HDH desalination – A review, Renew. Sustain. Energy Rev. 82 (2018) 629–644, http://dx.doi.org/10.1016/j.rser.2017.09.056.
[25] A. Fouda, S.A. Nada, H.F. Elattar, S. Rubaiee, A. Al-Zahrani, Performance analysis of proposed solar HDH water desalination systems for hot and humid climate cities, Appl. Therm. Eng. 144 (2018) 81–95, http://dx.doi.org/10.1016/j.applthermaleng.2018.08.037.
[26] Z. Zhao, H. Zheng, R. Jin, S. Liang, X. Ma, J. Zhao, Study of a compact falling film evaporation/condensation alternate-arrayed desalination system, Energy Convers. Manage. 244 (114511) (2021) 1–10, http://dx.doi.org/10.1016/j.enconman.2021.114511.
[27] D.U. Lawal, M.A. Antar, A. Khalifa, S.M. Zubair, F. Al-Sulaiman, Experimental investigation of heat pump driven humidification-dehumidification desalination system for water desalination and space conditioning, Desalination 475 (114199) (2020) 1–17, http://dx.doi.org/10.1016/j.desal.2019.114199.
[28] M. Schmack, G. Ho, M. Anda, A bubble column evaporator with basic flat-plate condenser for brackish and seawater desalination, Environ. Technol. 37 (1) (2016) 74–85, http://dx.doi.org/10.1080/09593330.2015.1063706.
[29] S.A. El-Agouz, A new process of desalination by air passing through seawater based on humidification–Dehumidification process, Energy 35 (12) (2010) 5108–5114, http://dx.doi.org/10.1016/j.energy.2010.08.005.
[30] A. Khalil, S.A. El-Agouz, Y.A.F. El-Samadony, A. Abdo, Solar water desalination using an air bubble column humidifier, Desalination 372 (Journal Article) (2015) 7–16, http://dx.doi.org/10.1016/j.desal.2015.06.010.
[31] M. Khan, M.A. Antar, A.E. Khalifa, S.M. Zubair, Experimental investigation of air heated bubble column humidification dehumidification desalination system, Int. J. Energy Res. (2020) 1–19, http://dx.doi.org/10.1002/er.5951.
[32] M. Preißinger, Bilge water treatment and desalination based on HDH-technology: an experimental investigation of a demonstration plant, Desalin. Water Treat. 127 (2018) 50–56, http://dx.doi.org/10.5004/dwt.2018.22532.
[33] M.T. Ghazal, U. Atikol, F. Egelioglu, An experimental study of a solar humidifier for HDD systems, Energy Convers. Manage. 82 (2014) 250–258, http://dx.doi.org/10.1016/j.enconman.2014.03.019.
[34] K. Srithar, T. Rajaseenivasan, Performance analysis on a solar bubble column humidification dehumidification desalination system, Process Saf. Environ. Prot. 105 (2017) 41–50, http://dx.doi.org/10.1016/j.psep.2016.10.002.
[35] E. Eder, M. Preißinger, Experimental analysis of the humidification of air in bubble columns for thermal water treatment systems, Exp. Therm Fluid Sci. 115 (110063) (2020) 1–8, http://dx.doi.org/10.1016/j.expthermflusci.2020.110063.
[36] Y. Katz, V. Dubovsky, G. Ziskind, R. Letan, Air-water transient heat transfer in a bubble column, in: HT2003, Heat Transfer: Volume 2, 2003, pp. 1–6, http://dx.doi.org/10.1115/HT2003-47165.
[37] E. Eder, S. Hiller, D. Brüggemann, M. Preißinger, Characteristics of air–liquid heat and mass transfer in a bubble column humidifier, Appl. Therm. Eng. 209 (2022) 118240, http://dx.doi.org/10.1016/j.applthermaleng.2022.118240.
[38] Deutsches Institut für Normung (DIN), DIN 38409: German Standard Methods for the Examination of Water, Waste Water and Sludge; General Measures of Effects and Substances (Group H); Determination of Hydrocarbons (H 18), Deutsches Institut für Normung, 1981.
[39] A. Savitzky, M.J.E. Golay, Smoothing and differentiation of data by simplified least squares procedures, Anal. Chem. 36 (8) (1964) 1627–1639, http://dx.doi.org/10.1021/ac60214a047.
[40] I. Aranberri, K.J. Beverley, B.P. Binks, J.H. Clint, P.D.I. Fletcher, How do emulsions evaporate? Langmuir 18 (9) (2002) 3471–3475, http://dx.doi.org/10.1021/la0115942.